7
Geometric Phase in Neutrino Oscillations

This chapter is based on the investigation acquired in Ref. [91]. In this chapter, the noncyclic geometric phase (GP) has been scrutinized in the three flavour neutrino oscillation framework where GP shows sensitivity to the neutrino mass ordering and CP-violation phase. In section 7.1, we spell out concept of noncyclic GP for a general state. Then, in section 7.2, we present the noncyclic GP for the neutrino system. The case of neutrinos propagating through vacuum has been discussed in section 7.2.1. The standard matter effects along with the effects of mass ordering and CP-violating phase have been demonstrated in section 7.2.2 where it is shown that observation of GP in neutrino-system can reveal the information on neutrino mass ordering. However, the issue of observation of GP in for neutrinos is still ponderable, hence an attempt is made to express GP in terms of observable neutrino oscillation probabilities. As both the GP and oscillation probabilities are functions of mixing angle θ and mass square difference Δ, the GP can be expressed in terms of survival and oscillation probabilities and their average values for two-flavour oscillations. This is shown explicitly in section 7.3.

7.1 Noncyclic geometric phase

Let us consider a state $|\chi(0)\rangle$ which evolves to a state $|\chi(t)\rangle$, after an arbitrary time t. Then, one can write the projection of state $|\chi(t)\rangle$ over $|\chi(0)\rangle$ such as $\langle\chi(0)|\chi(t)\rangle = r\, e^{i\Phi}$. The phase Φ here, has both dynamical and geometric parts. Since the dynamical phase depends on the energy of the system, it can be removed using gauge transformation, such as $|\psi\rangle \to |\tilde{\psi}\rangle = e^{i\xi}\,|\psi\rangle$ where $\xi = \frac{1}{\hbar}\int_0^t E(t')dt'$. However, the geometric part of the total phase still exists in the amplitude $\langle\chi(0)|\chi(t)\rangle$ even after the gauge transformation [78, 113]. Hence, the scalar product

$$\langle\chi(0)|\exp\left[\frac{i}{\hbar}\int_0^t \langle \mathrm{E}\rangle(t')dt'\right]|\chi(t)\rangle\,, \tag{7.1}$$

can be written as $r\, e^{i\beta}$, where r is a real number and angle β represents the noncyclic phase due to the evolution from $|\chi(0)\rangle$ to $|\chi(t)\rangle$ [78].

7.2 Noncyclic geometric phase in neutrino-system

We now consider three flavour oscillating neutrino states, $|\nu_\alpha(0)\rangle = U_{\alpha a}\,|\nu_a\rangle$, where $|\nu_\alpha(0)\rangle$ is initial flavour state (α = e, μ, τ) and $|\nu_a\rangle$ are mass eigenstates ($a = 1,\, 2,\, 3$). $U_{\alpha a}$ are the elements of the PMNS mixing matrix U.

The time evolution of $|\nu_\alpha\rangle$ in the flavour basis is given by

$$|\nu_\alpha(t)\rangle = U\, U_m(t)\, U^{-1}\,|\nu_\alpha(0)\rangle = U_f(t)\,|\nu_\alpha(0)\rangle\,. \tag{7.2}$$

$$U_m = \begin{pmatrix} e^{-i\omega_1 t} & 0 & 0 \\ 0 & e^{-i\omega_2 t} & 0 \\ 0 & 0 & e^{-i\omega_3 t} \end{pmatrix} \tag{7.3}$$

and $U_f(t) = U\, U_m(t)\, U^{-1}$.

To calculate the noncyclic phase generated during the time evolution of, say $|\nu_\mu(0)\rangle$ to $|\nu_\mu(t)\rangle$, we define a new state $|\tilde{\nu}_\mu(t)\rangle$, given by

$$|\tilde{\nu}_\mu(t)\rangle = \exp\left[i\int_0^t \langle \mathrm{E}\rangle(t')dt'\right]|\nu_\mu(t)\rangle\,, \tag{7.4}$$

where $\langle \mathrm{E}\rangle(t') = \langle\nu_\mu(t')|\, i\partial_t\, |\nu_\mu(t')\rangle$, and

$$|\nu_\mu(t')\rangle = U_{f12}(t')\,|\nu_e\rangle + U_{f22}(t')\,|\nu_\mu\rangle + U_{f32}(t')\,|\nu_\tau\rangle\,, \tag{7.5}$$

with $\langle\nu_\mu(0)|\nu_\mu(t')\rangle = U_{f22}(t')$, $U_{fab}(t')$ are a×b elements of the evolution operator U_f, $(a, b = 1, 2, 3)$. Then the scalar product is given by

$$\langle\nu_\mu(0)|\tilde{\nu}_\mu(t)\rangle = \exp\left[i\int_0^t \langle \mathrm{E}\rangle(t')dt'\right]\; U_{f22}(t') \equiv r_{\mu\mu}e^{i\beta_{\mu\mu}}, \tag{7.6}$$

so that the noncyclic phase due to evolution from $|\nu_\mu(0)\rangle$ to $|\nu_\mu(t)\rangle$ will be the phase angle $\beta_{\mu\mu}$. Similarly, it is possible to compute the other inner products, such as, $\langle\nu_\mu(0)|\tilde{\nu}_e(t)\rangle$ and their corresponding noncyclic phases.

7.2.1 Non cyclic geometric phase in vacuum

Using the definition of non-cyclic GP from the previous section, the theoretical expressions of GP, such as β_{ee}, $\beta_{e\mu}$, $\beta_{\mu\mu}$ and $\beta_{\mu e}$, are [78]

$$\begin{aligned}\beta_{ee} &= (2s_{12}^2c_{13}^2 + 2qs_{13}^2 - 1)(\phi\frac{L}{c}) \\ &\quad + \tan^{-1}\frac{\cos(2\theta_{12})c_{13}^2\sin(\phi\frac{L}{c}) - s_{13}^2\sin[(2q-1)\phi\frac{L}{c}]}{c_{13}^2\cos\phi\frac{L}{c} + s_{13}^2\cos[(2q-1)\phi\frac{L}{c}])},\end{aligned} \tag{7.7}$$

$$\begin{aligned}\beta_{e\mu} &= \big[\cos(2\theta_{12})(c_{23}^2 - s_{13}^2s_{23}^2) + c_{13}^2s_{23}^2(2q-1) - s_{13}\sin(2\theta_{12})\sin(2\theta_{23})\cos(\delta)\big](\phi\frac{L}{c}) \\ &\quad + \tan^{-1}\frac{s_{13}s_{23}[s_{12}^2\sin(\phi\frac{L}{c}+\delta) - c_{12}^2\sin(\phi\frac{L}{c}-\delta) - \sin\psi_+] - c_{23}\sin(\phi\frac{L}{c})\sin(2\theta_{12})}{\sin(\theta_{13})\sin(\theta_{23})[cos\psi_+ - s_{12}^2\cos(\phi\frac{L}{c}+\delta) - c_{12}^2\cos(\phi\frac{L}{c}-\delta)]},\end{aligned} \tag{7.8}$$

$$\begin{aligned}\beta_{\mu\mu} &= \big[\cos(2\theta_{12})(c_{23}^2 - s_{13}^2s_{23}^2) + c_{13}^2s_{23}^2(2q-1) - s_{13}\sin(2\theta_{12})\sin(2\theta_{23})\cos\delta\big](\phi\frac{L}{c}) \\ &\quad + \tan^{-1}\frac{s_{13}\sin(2\theta_{12})\sin(2\theta_{23})\cos\delta\sin(\phi\frac{L}{c}) - (c_{23}^2 - s_{23}^2s_{13}^2)\cos(2\theta_{12})\sin(\phi\frac{L}{c}) - c_{13}^2s_{23}^2\sin\Gamma}{(c_{23}^2 + s_{13}^2s_{23}^2)\cos(\phi\frac{L}{c}) + c_{13}^2s_{23}^2\cos\Gamma},\end{aligned} \tag{7.9}$$

$$\begin{aligned}\beta_{\mu e} &= (2s_{12}^2c_{13}^2 + 2qs_{13}^2 - 1)(\phi\frac{L}{c}) \\ &\quad + \tan^{-1}\frac{s_{13}s_{23}[s_{12}^2\sin(\phi\frac{L}{c}-\delta) - c_{12}^2\sin(\phi\frac{L}{c}+\delta) - \sin\psi_-] - c_{23}\sin(\phi\frac{L}{c})\sin(2\theta_{12})}{\sin(\theta_{13})\sin(\theta_{23})[\cos\psi_- - s_{12}^2\cos(\phi\frac{L}{c}-\delta) - c_{12}^2\cos(\phi\frac{L}{c}+\delta)]},\end{aligned} \tag{7.10}$$

where $q = (\omega_3 - \omega_1)/(\omega_2 - \omega_1) = (\Delta m_{32}^2/\Delta m_{21}^2) + 1$; $\phi = \Delta m_{21}^2/4E\hbar$; $\Gamma = (2q-1)(\phi L/c)$ and $\psi_\pm = (2q-1)(\phi L/c) \pm \delta$. Further, L is the propagation length and E is the neutrino energy.

For the cyclic case scenario, q would be a rational number with the cyclic period $t = 2\pi/(\omega_1 - \omega_2)$ [75, 78].

In our analysis, the values of mixing angles, θ_{ij}, and mass square differences, $\Delta m^2_{ij} = m^2_i - m^2_j$ (m_i and m_j are the masses of the neutrino mass eigenstates ν_i and ν_j, respectively), used are $\theta_{12} = 33.48^o$, $\theta_{13} = 8.5^o$, $\theta_{23} = 42.3^o$, $\Delta m^2_{21} = 7.5 \times 10^{-5} eV^2$, Δm^2_{31} ($\approx \Delta m^2_{32}$) $= \pm 2.457 \times 10^{-3} eV^2$. The plots of $\beta_{\mu\mu}$ and $\beta_{\mu e}$ with respect to L (for two cycles) for neutrino energy E = 1 GeV for different values of δ are shown in Fig. 7.1. As can be seen from the figure, for $\beta_{\mu\mu}$, there is mild (almost negligible) dependence on δ whereas $\beta_{\mu e}$ is significantly sensitive to δ. Similarly, we find that $\beta_{e\mu}$ is sensitive to the CP phase whereas β_{ee} is not. Therefore in order to study the effect of CP violating phase on GP, we consider $\beta_{e\mu}$ and $\beta_{\mu e}$ in this work.

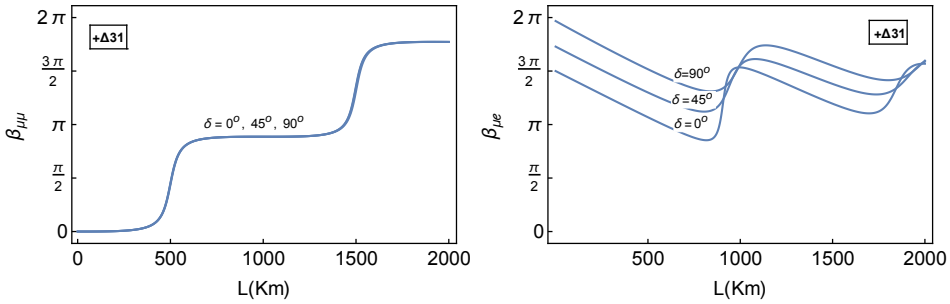

Figure 7.1: The top and bottom figures show the variation of $\beta_{\mu\mu}$ and $\beta_{\mu e}$ with L (in Km), respectively in vacuum for different values of δ. Here neutrino energy E = 1 GeV.

7.2.2 Non cyclic geometric phase in the presence of earth matter effects

In order to calculate non-cyclic GP in the presence of matter, we make use of the formalism given in [127, 128, 219]. In this formalism, the evolution operator which evolves an initial flavour state, in mass eigenstate basis and flavour state basis in a constant matter density are given by

$$U_m(L) = \phi \sum_{a=1}^{3} \frac{e^{-iL\lambda_a}}{3\lambda_a^2 + c_1}[(\lambda_a^2 + c_1)I + \lambda_a T + T^2], \tag{7.11}$$

$$U_f(L) = \phi \sum_{a=1}^{3} \frac{e^{-iL\lambda_a}}{3\lambda_a^2 + c_1}[(\lambda_a^2 + c_1)I + \lambda_a \tilde{T} + \tilde{T}^2], \tag{7.12}$$

respectively. The T matrix has the form

$$\mathbf{T} = \begin{pmatrix} AU_{e1}^2 - \frac{1}{3}A + \frac{1}{3}(E_{12} + E_{13}) & AU_{e1}U_{e2} & AU_{e1}U_{e3} \\ AU_{e1}U_{e2} & AU_{e2}^2 - \frac{1}{3}A + \frac{1}{3}(E_{21} + E_{23}) & AU_{e2}U_{e3} \\ AU_{e1}U_{e3} & AU_{e2}U_{e3} & AU_{e3}^2 - \frac{1}{3}A + \frac{1}{3}(E_{31} + E_{32}) \end{pmatrix}, \tag{7.13}$$

with $\phi = e^{\frac{-i}{3}LTr\mathcal{H}_m}$, $T = \mathcal{H}_m - Tr[\mathcal{H}_m]/3$, $c_1 = \det T\ Tr(T^{-1})$ and λ_a are eigenvalues of T, matter potential $A = \pm\sqrt{2}\, G_F\, n_e$ (+ for neutrinos, - for anti-neutrinos), G_F is Fermi constant, n_e is the electron number density, $E_{ij} = E_i - E_j$ and $\tilde{T} = UTU^{-1}$.

If neutrinos travel through a series of constant matter densities, say A_1, A_2, A_3,...A_n, and evolution operators corresponding to these matter densities are U_1, U_2, U_3,.....U_n then $U' = U_1U_2U_3....U_n$. For Earth's mantle-core-mantel step function density profile, with U_1 and U_2 corresponding to mantle and core of the Earth respectively, U' will become $U' = U_1U_2U_1$. The changes in the evolution operator translate into corresponding changes in the noncyclic phases.

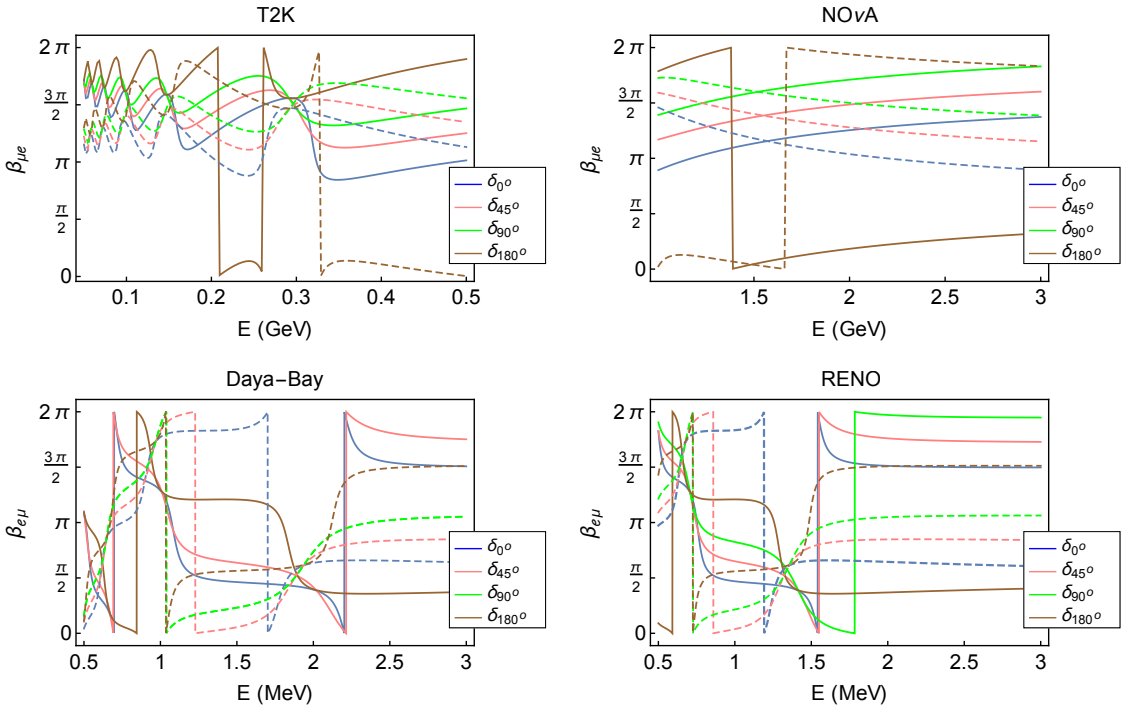

Figure 7.2: First and second figures from top depict $\beta_{\mu e}$ vs E (GeV) plots for T2K and NOνA experimental set-ups, respectively whereas the third and fourth figures show the variation of $\beta_{e\mu}$ with E (MeV) for Daya-Bay and RENO set-ups, respectively for different CP-violating phases $\delta = 0$ (blue), $\delta = \frac{\pi}{4}$ (pink), $\delta = \frac{\pi}{2}$ (green) and $\delta = \pi$ (brown). Solid and dashed lines in these plots correspond to positive and negative signs of Δm^2_{31}, respectively.

We now study GP for neutrinos produced at various man made facilities such as the reactor and accelerator neutrino experiments. For reactor neutrinos, we consider Daya-Bay and RENO experimental set-ups whereas for accelerator neutrinos, we present results for NOνA and T2K. Daya-Bay is a China based reactor neutrino experiment[204, 220] which uses a cluster of six nuclear reactors to get $\bar{\nu}_e$ anti-neutrinos with energy range of MeV order and three detectors are placed at distance of units of Km. One far detector is placed at approximately 2 Km distant from the source. This baseline has to face the constant rock matter density with matter potential A = -1.01×10^{-13} eV (negative sign due to $\bar{\nu}_e$). RENO is also a reactor $\bar{\nu}_e$-experiment. Its baseline is 1.4 Km with energy range in units of MeV. Since initial flavour state in these experiments are $\bar{\nu}_e$, therefore we analyze $\beta_{e\mu}$ component of the GP.

Accelerator neutrino-experiment NOνA experiment uses NuMi-beam of accelerator ν_μ-neutrinos based at Fermilab [199, 201]. The detector is 810 Km (baseline) distant from the source of ν_μ neutrinos in the energy range of 1-10 GeV. Its aim is to measure the small mixing angle θ_{13}, the neutrino-mass ordering and the CP-violating phase. This baseline passes through the Earth's crust which has a constant matter density 1.7×10^{-13} eV. T2K is an off-axis experiment [194, 197] which uses a ν_μ- neutrino beam from Tokai to Kamioka with energy-range of approximately 100 MeV to 1 GeV. It has 295 Km long baseline and passes through a matter density of 1.01×10^{-13} eV. For accelerator neutrinos, we consider $\beta_{\mu e}$ component of GP.

Figure 7.2 shows the variation of $\beta_{e\mu}$ (for Daya-Bay and RENO) and $\beta_{\mu e}$ (for T2K and NOνA) with neutrino energy, E, for different values of CP violating phase δ for initial anti electron neutrino and muon neutrino beams, respectively. It can be seen from the figure that T2K, Daya-Bay and RENO have neutrino energies and baselines such that the GP can complete at least

one cycle. This is because of the factor *(2q-1)*$\phi = (\frac{\Delta m^2_{32}+\Delta m^2_{31}}{4E\hbar c}) = (\frac{2\Delta m^2_{32}+\Delta m^2_{21}}{4E\hbar c})$, in Eqs. (7.8) and (7.10), which plays a leading role in the oscillatory nature of the GP. In accordance with this factor, the value of L/E, corresponding to one cycle, should be $\left(\frac{L}{E}\right)_{req} \sim 0.99$ Km/MeV for $+\Delta m^2_{31}$ and ~ 1.03 Km/MeV for $-\Delta m^2_{31}$. While, the value of L/E is 2950 Km/GeV (2.95 Km/MeV) for T2K (at L = 295 Km, E = 100 MeV), 2 Km/MeV for Daya-Bay (at L = 2 Km, E = 1 MeV) and 1.4 Km/MeV for RENO (at L = 1.4 Km, E = 1 MeV) which is greater than the required L/E value for one cycle, the value of L/E for NOνA (at L = 810 Km, E = 1 GeV) $\sim$ 810 Km/GeV (0.81 Km/MeV) is not enough to have at least one cycle. These L/E values for specific experimental set-ups are calculated at their corresponding lowest energy-values of neutrinos and the baseline length.

Further, we find that for L/E corresponding to a cycle, all GP curves corresponding to different values of CP-phase, converge to a single point. We call this point as *cluster point*. This is so because in the limit $\phi\frac{L}{c} \to \frac{2\pi}{(2q-1)}$, i.e., where one cycle of oscillating feature of GP gets completed, $\beta_{e\mu}$ remains approximately constant for every CP violating phase δ. An interesting thing to observe here is that there are two distinct cluster points corresponding to + and - signs of Δm^2_{31}. This would thus help in removing the sign ambiguity in Δm^2_{31}. Therefore if we choose proper energy range, for the fixed baseline length, such that L/E corresponds to a cycle of the GP, then one can disentangle effects of + and - signs of Δm^2_{31}. For example, for the case of Daya-Bay experiment (L = 2 km), we are getting these cluster points at E = 1 MeV and 2 MeV. So one has to tune the energy value of anti-neutrinos at these values and by measuring the GP-value, the effect of + and - signs can be disambiguated.

As the baseline length and energies for experiments such as Daya-Bay, RENO and T2K allows at least one complete cycle of GP, measurement of GP of neutrinos with energy within specific energy range (such that condition for cluster point is satisfied) can enable resolving the sign ambiguity in Δm^2_{31}. This can be seen from Fig. 7.3 where predictions for GP for both signs of Δm^2_{31} are shown for various experimental set-ups. Here L for these set-ups are fixed at their baseline length and E is selected so that L/E corresponds to one cycle of GP. It is obvious from the figure that the predictions for GP are different for + and - signs of Δm^2_{31} and hence one can determine the sign of Δm^2_{31}. For Daya-Bay, the predictions for both signs of Δm^2_{31} are different for all values of CP violating phase for E between (0.95 - 1.02) MeV and (1.97 - 2.04) MeV with L fixed at the baseline length.

For RENO (T2K), the predictions for both signs of Δm^2_{31} are different for neutrino energy range (1.38 - 1.42) MeV ((95 - 101) MeV). In Fig. 7.3 dashed and dotted curves represent the case of the lowest and the highest limits of these energy ranges, respectively. Solid curves correspond to that specific energy value at which a cycle of GP gets completed (eg. for RENO, solid curve correspond to E = 1.4 MeV). Hence measurement of GP would be helpful in resolving the degeneracy in Δm^2_{31}. The points in Fig. 7.3 where all three curves representing different values of energy, for specific sign of Δm^2_{31}, intersect because at the value of CP-phase, corresponding to intersection point (say $\delta \sim 195^o$ for RENO), the value of GP remains constant in the energy range mentioned above for different experimental set-ups.

The incapability of the NOνA experimental setup in distinguishing the effects of normal and inverted mass ordering on GP is observed due to its corresponding lower L/E value than the required L/E value for complete one cycle, i.e., $\left(\frac{L}{E}\right)_{NO\nu A} \leq \left(\frac{L}{E}\right)_{req}$. However, the higher energy of neutrinos associated to NOνA (1-10 GeV) makes it a bit different from the other ones such as T2K (0.1-1 GeV), Daya Bay & RENO (1-10 MeV) due to significant matter effect (the higher is the neutrino-energy, the higher would be the neutrino-matter interaction). Hence, we investigated the GP for energy $E = 1$ GeV and the baseline which is extended up to around 5000 Km. We could observe in Fig. 7.4 that in vacuum-case (left), both of the branches, corresponding to $+$ sign

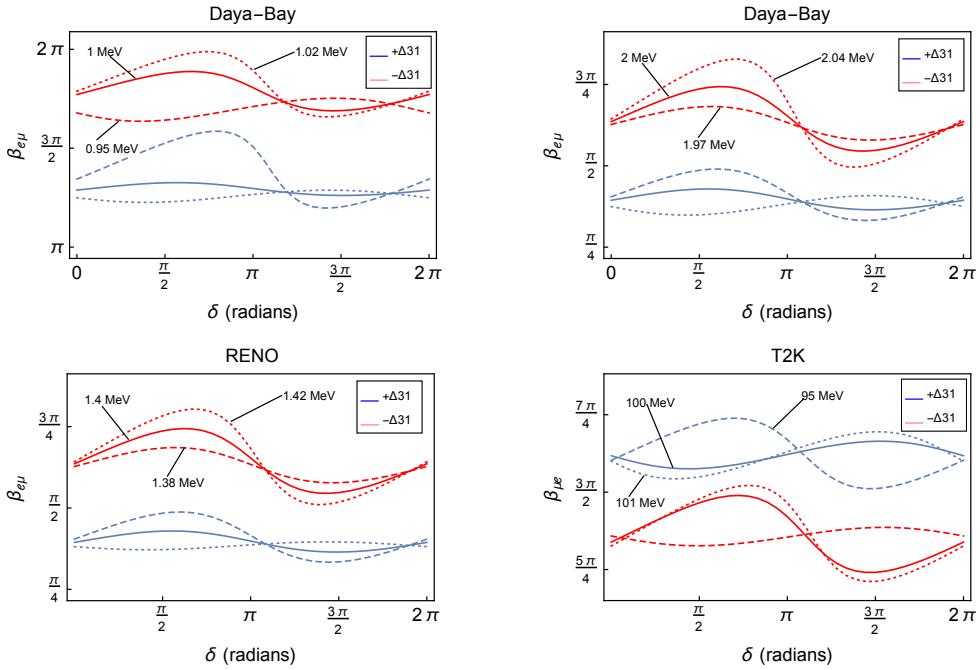

Figure 7.3: From top, the first and second figures show $\beta_{e\mu}$ vs δ plots for Daya-Bay experimental set-up. The third and fourth figures show variation of $\beta_{e\mu}$ and $\beta_{\mu e}$ with δ, for RENO and T2K experimental set-ups, respectively. Solid curves in these plots correspond to that specific value of neutrino energy at which a cycle of GP gets completed. The solid curves in first and second figures, for Daya-Bay, correspond to 1 and 2 MeV, respectively. The solid curve for RENO and T2K correspond to 1.4 and 100 MeV, respectively. Dashed and dotted curves correspond to lower and upper limits of neutrino energies for which the GP predictions for both signs of Δm^2_{31} are different. Blue and red curves correspond to predictions for positive and negative signs of Δm^2_{31}, respectively.

(solid curves) and $-$ sign (dashed curves) are getting separated after a long distance traveled by neutrinos. But in case of matter effect (right), the separation has not been observed.

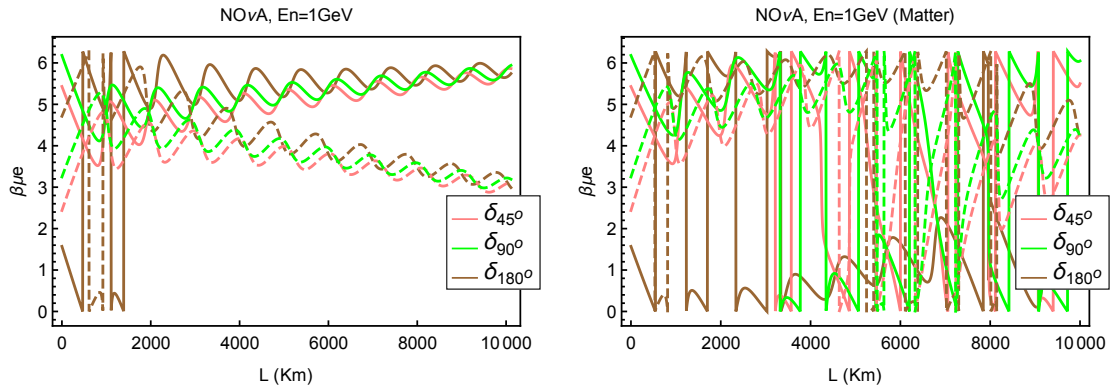

Figure 7.4: $\beta_{\mu e}$ **Vs. L:** This figure shows the variation of $\beta_{\mu e}$ with respect to L at $\delta = 90^o$. Left and right figures correspond to $+$ and $-$ signs of Δm^2_{31}, respectively.

7.3 Geometric phase in terms of survival and oscillation probabilities

Experimental detection of GP usually makes use of interference set-ups. However, in the case of neutrinos, this would not be feasible [188, 221]. Nevertheless, one could envisage an interference experiment in energy space. This idea was used in [81] to show, in the context of two-flavour neutrino oscillations, that the topological (Pancharatnam) phase of the interference term was implicit in the transition probabilities associated with the neutrino oscillations. It was seen to be a consequence of the orthogonality of the two-flavour PMNS matrix. The analysis was made by exploiting the analogy between the geometry of two-state neutrino system and polarization states in optics.

The currently running experiments related to neutrino oscillations are designed to measure only survival ($P_{\alpha\alpha}$) or oscillation ($P_{\alpha\beta}$) probabilities. Hence in order to measure geometric phase, it should be expressed in terms of these experimentally measurable quantities. This can be illustrated in a simple way by working within the context of two flavour neutrino oscillations. The probabilities are given by

$$P_{ee} = 1 - \sin^2(2\theta)\,\sin^2(\frac{\Delta L}{4E\hbar c}), \tag{7.14}$$

$$P_{e\mu} = \sin^2(2\theta)\,\sin^2(\frac{\Delta L}{4E\hbar c}). \tag{7.15}$$

Here, we have neglected the matter effect for simplicity. In the context of two flavour neutrino oscillations, Eqs. (7.7), (7.8), (7.9), (7.10) reduce to

$$\beta_{ee} = -\phi t\cos(2\theta) + \tan^{-1}[\cos(2\theta)\tan(\phi t)], \tag{7.16}$$

$$\beta_{e\mu} = \phi t\cos(2\theta) - \frac{\pi}{2}, \tag{7.17}$$

$$\beta_{\mu\mu} = \phi t\cos(2\theta) - \tan^{-1}[\cos(2\theta)\tan(\phi t)], \tag{7.18}$$

$$\beta_{\mu e} = -\phi t\cos(2\theta) - \frac{\pi}{2}. \tag{7.19}$$

Using Eqs. (7.14)- (7.19), the components of geometric phase can be written in terms of neutrino survival or oscillation probability and their average values:

$$\begin{aligned}\beta_{ee}\big(P_{ee},\langle P_{ee}\rangle\big) = &-\frac{1}{2}\cos^{-1}\left[\frac{P_{ee}-\langle P_{ee}\rangle}{1-\langle P_{ee}\rangle}\right]\sqrt{2\langle P_{ee}\rangle - 1}\\ &+\tan^{-1}\left[\sqrt{2\langle P_{ee}\rangle - 1}\,\tan\left(\frac{1}{2}\cos^{-1}\left[\frac{P_{ee}-\langle P_{ee}\rangle}{1-\langle P_{ee}\rangle}\right]\right)\right],\end{aligned} \tag{7.20}$$

$$\beta_{e\mu}\big(P_{e\mu},\langle P_{e\mu}\rangle\big) = \frac{1}{2}\cos^{-1}\left[1-\frac{P_{e\mu}}{\langle P_{e\mu}\rangle}\right]\sqrt{1-2\langle P_{e\mu}\rangle} - \frac{\pi}{2}, \tag{7.21}$$

$$\begin{aligned}\beta_{\mu\mu}\big(P_{\mu\mu},\langle P_{\mu\mu}\rangle\big) = &\frac{1}{2}\cos^{-1}\left[\frac{P_{\mu\mu}-\langle P_{\mu\mu}\rangle}{1-\langle P_{\mu\mu}\rangle}\right]\sqrt{2\langle P_{\mu\mu}\rangle - 1}\\ &-\tan^{-1}\left[\sqrt{2\langle P_{\mu\mu}\rangle - 1}\,\tan\left(\frac{1}{2}\cos^{-1}\left[\frac{P_{\mu\mu}-\langle P_{\mu\mu}\rangle}{1-\langle P_{\mu\mu}\rangle}\right]\right)\right],\end{aligned} \tag{7.22}$$

$$\beta_{\mu e}\big(P_{\mu e},\langle P_{\mu e}\rangle\big) = -\frac{1}{2}\cos^{-1}\left[1-\frac{P_{\mu e}}{\langle P_{\mu e}\rangle}\right]\sqrt{1-2\langle P_{\mu e}\rangle} - \frac{\pi}{2}. \tag{7.23}$$

Here $\langle P_{\alpha\beta}\rangle$ is the average value of probability $P_{\alpha\beta}$ and is given by

$$\langle P_{\alpha\beta}\rangle = \begin{cases} 1-\frac{\sin^2(2\theta)}{2} & \text{for } \alpha=\beta \\ \frac{\sin^2(2\theta)}{2} & \text{for } \alpha\neq\beta \end{cases}$$

Thus we see that phases associated with neutrino oscillations can be expressed in terms of the experimentally measurable quantities.

There are several theoretical analyses of GP in context of neutrino oscillation. For example, pointing out the existence of distinct versions (or generalizations) of GP in the standard Pontecorvo formulation of neutrino mixing while neutrino is traveling in vacuum or material medium and also some of its applications as discriminating the Dirac or Majorana nature of neutrinos and many such others. However, none of these studies have commented on the observational issues of GP in neutrino sector. An ideal way of observing GP is to setup a split-beam experiment. In optical systems, it can be done using the refractive and reflective properties of the medium and accordingly, one can setup lenses and mirrors to separate a beam into two parts and then, to let these beams interfere. Since, these beams traverse through different paths, a relative phase shift can be observed after their interference. However, in case of neutrinos, the refractive index is very small ($n_{eff} - 1 \approx 10^{-19}$ in normal matter for neutrinos of 1 MeV energy). One can treat our Sun, which has its core density ≈150 gm/cc, as a neutrino-lens whose focal length comes out to be $10^{18} R_{\odot}$ for a neutrino of energy around 10 MeV, which is 10^5 times the size of our milky way galaxy [222]. Hence, it can be considered impossible to arrange a two-neutrino-beam-experiment for such observation of GP. Moreover, neutrino oscillation, say two-flavour oscillation, itself is a consequence of an interference phenomenon where two mass eigenstates separately propagate in the energy space acting like two beams and then interfere with each other to produce a neutrino state of same or different flavour. This idea is also discussed in [81].

In presence of such complexities, it is not possible to do a direct measurement of GP in case of neutrinos. However, here we have expressed GP in terms of neutrino oscillation probabilities, only observable quantities in the neutrino sector. This furnishes a platform for an indirect observation of GP in neutrino oscillation experiments.